Dekameter Radar Observations of Ocean Wave Growth and Decay

ROBERT H. STEWART

Scripps Institution of Oceanography, University of California, San Diego 92093

CALVIN TEAGUE

Center for Radar Astronomy, Stanford University, Stanford, CA 94305

(Manuscript received 19 February 1979, in final form 24 August 1979)

ABSTRACT

Immediately following the passage of polar fronts that produced strong winds blowing away from Galveston Island and into the Gulf of Mexico, we used scattered LORAN-A radio waves, together with observations by wave staffs, to measure the growth of 80 m waves as a function of angle to the wind, and the decay of the same wavelengths going against the wind. The LORAN signals at 2 MHz are in Bragg resonance with 80 m (7 s) ocean waves offshore, and were used to map the strength of both approaching and receding 80 m waves as a function of range and azimuth using Doppler velocity to determine wave directions. We found that 1) these waves grow as the cosine of the angle to the wind; 2) growth rates averaged over all angles are comparable to those previously published; 3) growth rates measured as a function of time by the wave staff were numerically the same as growth measured as a function of distance by the radar; 4) growth appears to be inhibited for waves having frequencies near the peak frequency of preexisting waves going against the wind, but apparently not at higher frequencies; 5) attenuation of waves going against the wind is very weak compared with growth rates under the same conditions; and 6) ~1% of wave energy incident on a very gently sloping natural beach is reflected back to sea.

1. Introduction

Prediction of oceanic wave heights has long been a fundamental goal in oceanography, and a primary reason for studying wave behavior. While considerable progress has been made, the problem is not yet completely solved.

Sverdrup and Munk (1947) formulated the first successful approach to predicting waves by considering the behavior of significant waves, those waves apparent to an observer near the sea surface. Using an existing body of wave observations, they showed that wave height, period and wavelength increased with the duration of the wind, or with fetch, the distance over which the wind blew, and that this increase was predictable.

Their empirical approach, while successful, was not entirely satisfying. It was soon argued that the significant wave was a false construction, and that in reality, the sea surface was composed of a superposition of many different wavelengths going in a variety of directions relative to the wind. This concept of a spectrum of ocean waves recast the problem of wave prediction into predicting the behavior of each individual component in the spectrum.

Studies of the wave spectrum soon dominated, and have continued for the last two decades. But despite their preceived importance, ocean wave studies have really been relatively few. It is difficult to build and deploy special instruments to measure wave height and frequency, let alone wave direction, and the weather at sea is seldom suitable for controllable experiments. Constant winds with known duration and fetch are usually rare or hard to find.

Pierson and Moskowitz (1964), in their study of the shape of the spectrum, searched through years of data and more than 1000 wave records before they found 54 suitable for their analysis. They and others showed that the spectrum was narrow band, i.e., wave energy is confined to a relatively narrow band of frequencies near the peak, and that at relatively great fetches or times, the spectra produced by various winds were of similar shape. Snyder and Cox (1966) and Barnett and Wilkerson (1967) studied the growth of components of wave spectra as the wind blew away from a lee shore, and Inoue (1966) studied wave growth with time in the central North Atlantic. The former found an initial period of linear growth quickly followed by exponential growth; and all found that the rate of exponential growth was a weak function of wind velocity relative to the phase velocity of the wave components they studied.

Measurements made during the Joint North Sea Wave Project (JONSWAP) reestablished the original view of wave prediction, although on a firmer

0022-3670/80/010128-16$08.00

theoretical basis. The frequency spectrum of waves growing away from a lee shore was found to be self-similar in shape, although not quite the same shape as the spectrum of Pierson and Moskowitz, and that it could be described by a few parameters, notably total wave energy, the frequency at the peak, and the relative energy of shorter wavelengths (Hasslemann *et al.*, 1973). These parameters changed in a predictable way with fetch and wind speed, and the shape of the spectrum was self-preserving under the influence of interactions among various wave components in the spectrum. Once again wave prediction depended on knowing only how the parameters of the spectrum vary with fetch or duration; and there is little difference between these new parameters (for example, the period of waves at the peak in the spectrum) and the old variables such as significant wave period.

While the JONSWAP ideas go a long way toward explaining the development of the sea, some information is still lacking. Is the directional distribution of the sea self-similar or how does wave growth vary with angle to the wind? What is the influence of existing waves on the growing wave field? And how fast are waves flattened by an opposing wind? To help answer these questions we sought to observe wave growth away from a lee shore during periods of steady winds. Ideally, we wanted a steady onshore wind that suddenly reversed and then blew steadily offshore. This would allow us to observe both the growth of a new field of waves and the decay of the old field.

Because of high cost, it was not practical to measure the wave field using instruments on the surface spaced out along a line of increasing fetch. Rather, we used a technique, developed at Wake Island, which uses scattered radio waves to measure the energy density of a single wave component along lines projecting radially away from a point on shore (Tyler *et al.*, 1974; hereafter referred to as TTSPMJ). From these measurements we are able to observe the growth of this component as a function of angle to shore, the influence of existing waves on this growth, and the decay of waves components having the same wavelength but going against the wind.

The general plan of the experiment and the techniques for measuring waves and the weather are described in the next sections. Then we describe the observations and, in the last section, we examine their implications.

2. Data sets and analysis

a. Site of the experiment

The measurements were made offshore of Galveston Island, a low barrier island along the Texas coast in the Gulf of Mexico. There, moderate winds usually blew toward the shore from the south or southeast but a number of times during the winter of 1976, strong cold fronts crossed the area. After passage of the fronts the wind blew strongly from the north-northwest nearly perpendicular to the shore for a day or so, then gradually weakened and shifted toward the east.

The island and the adjacent Texas coast are very straight and low, and do not disrupt the flow of wind (Fig. 1a). Offshore the water quickly deepens to 18–20 m at a distance of 20 km from the shore, and remains at nearly this depth out to 60 km where it continues to deepen. We expect that these depths have little influence on the 80 m waves we wish to measure. Their phase velocity is

$$c^2 = g/k \tanh(kh),$$

where $k = 2\pi/(80\text{ m})$ is the wavenumber, g is gravity and h the water depth. Using typical depths, we find that beyond 20 km, 80 m waves are slowed no more than 7%, and beyond 60 km, where most wave growth occurs, they are slowed by less than 2% (Fig. 2).

The island was also a suitable base for the radar measurements. A LORAN-A station, located on the northeast tip of the island, served as a source of high-power radio pulses, and we could drive along numerous straight roads and a long hard beach in order to synthesize high-resolution directional antennas. Offshore, several complexes of oil and gas producing platforms served as suitable locations for auxilliary wind and wave measurements.

b. The wave measurements

The primary source of wave data were observations of radio signals scattered from 80 m (7 s) ocean waves using the synthetic-aperture technique described in TTSPMJ. The LORAN-A radio station transmits 50 μs pulses of 160 m (1.95 MHz) vertically polarized radio waves. These propagate out over the water, and because of their long wavelength, they follow the earth's curvature and travel well beyond the horizon. There they are resonantly backscattered by those components of the ocean-wave spectrum that match the equations for Bragg scatter, that is, by those waves that are exactly one-half the radio wavelength and that propagate radially toward or away from the radar; other waves have no influence on the scatter. The scattered power is directly proportional to the energy density of the scattering ocean waves, and the scattered frequency is Doppler-shifted by exactly the frequency of the ocean wave component.

This description of the scatter of radio waves from the sea is based on the theory of Rice (1951) as interpreted by Barrick (1972), and is well established by experiments (Barrick *et al.*, 1974; Teague *et al.*,

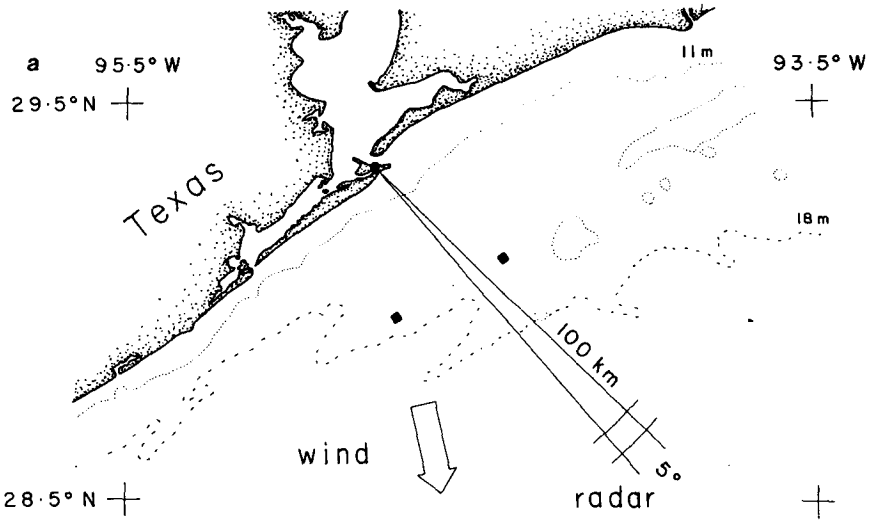

FIG. 1a. The Texas Gulf coast, showing the location of the LORAN-A transmitter on the tip of Galveston Island (solid circle), the location of the offshore wave staffs (solid squares) and water depths. The radar beam is drawn to scale and shows the approximate size of the radar scatter area.

1977). It is essentially the same as the scatter of light from a diffraction grating or x-rays from a crystal lattice. To be applicable, the theory requires that the radio wavelength be much greater than the height of the ocean surface roughness, and that the surface be highly conducting. Both conditions are well satisfied for our experiment, where 160 m radio waves were scattered from 80 m waves only a few meters high. At higher radio frequencies, the first condition is not always met, and second-order scatter, sometimes observed in other experiments, becomes important.

In the experiment, the radio signals were received by a very directional synthesized antenna (described below) and were used to map the wave field offshore. By observing the time for pulses to go out and back, we obtained the range to the scattering area; and by observing the azimuthal direction from which they are received, we obtained the angle to the scattering area. Typically, this area was 7.5 km in range by 5° wide (Fig. 1a), and scatter was observed out to ranges of several hundred kilometers.

An antenna with a beamwidth of 5° requires an aperture of 10 wavelengths, i.e., 1.6 km in length.

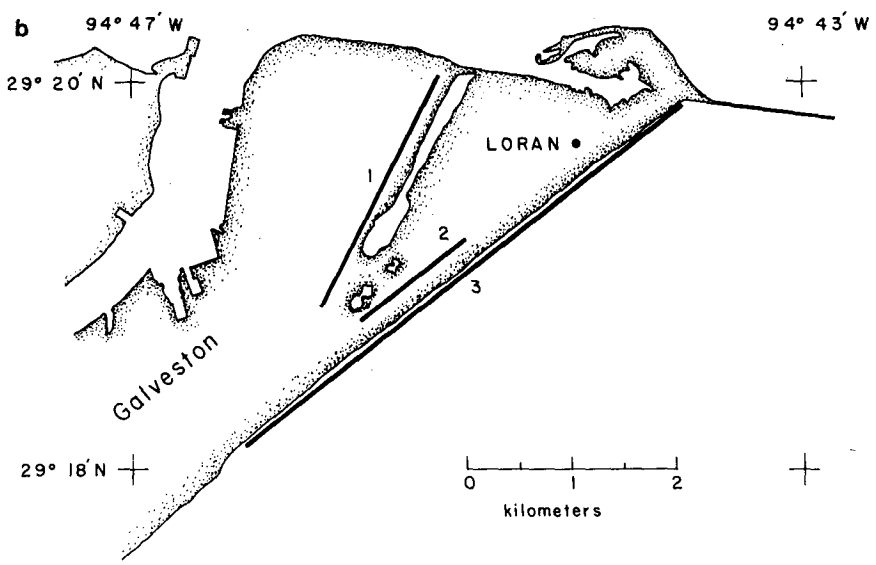

FIG. 1b. The paths used to synthesize a directional antenna. 1, Seawall Boulevard; 2, East Beach Road; 3, the beach just below high tide level, exposed by winds blowing offshore.

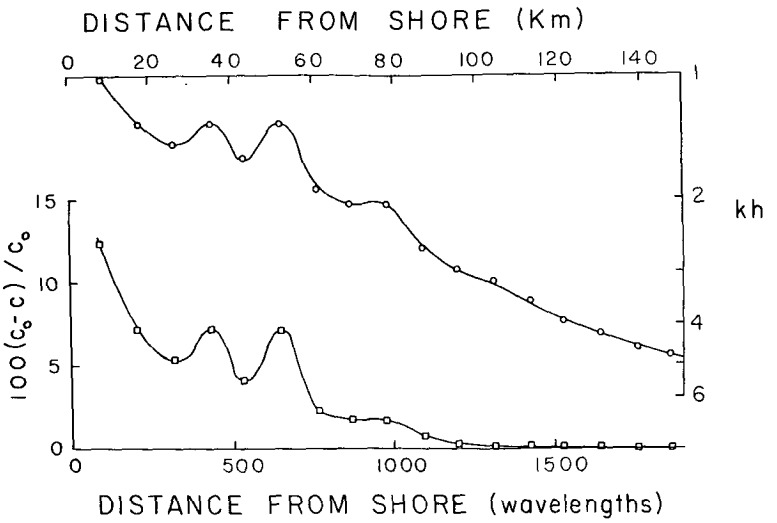

FIG. 2. The influence of bottom at depth h on the 80 m waves of wavenumber k observed by the radar. kh is the dimensionless depth as a function of distance from shore, c_0 the phase velocity of 80 m waves in deep water, and c their velocity in depth h. Both horizontal scales are the same, but are expressed in different units.

To form such a narrow beam antenna, we synthesized a large aperture by continuously recording the signal from a receiver driven at constant velocity along straight paths several kilometers in length near the transmitter (Fig. 1b). Normally, the frequency spectrum of the backscattered signal recorded by a stationary receiver contains three lines, two at ±0.14 Hz due to the approaching and receding components of the ocean-wave spectrum, and one due to land. If the receiver moves at constant velocity, the motion produces an additional Doppler shift which depends on the angle between the velocity vector and the direction to the scattering area. Thus the strength of the received signal at each frequency interval in the Doppler spectrum of the scattered radio signal can be related to the energy density of waves traveling at a particular azimuthal angle. The effective aperture is the distance traveled by the receiver, and this determines the azimuthal resolution. The velocity is arbitrary, but to keep separate the three bands in the spectrum, it should be less than 11.1 m s^{-1}, the phase velocity of the scattering waves. Typically we drove a small van equipped with speed-controlling device at 7 m s^{-1} along straight sections of road or along the beach (Fig. 1b) to synthesize antennas with apertures of 1–3 km and azimuthal resolutions of 3–10°.

To obtain statistically reliable estimates of ocean wave energy density, and to reduce noise, many independent radio observations were averaged together. This was done in several ways. First, each scattered pulse was digitized every 25 μs to an accuracy of 0.4% (8 bits), and eight consecutive pulses, which were transmitted at a rate of 35 s^{-1}, were averaged together to obtain one point every 0.24 s in the time history of scatter at each of 128 ranges. During this 0.25 s interval, scatter from the sea is stationary, and the average reduces noise by a factor of $\sqrt{8}$. Next the time series for each traverse of the antenna path were Fourier transformed to obtain the Doppler spectrum at each range, and the scatter was separated into azimuthal directions of approaching and receding waves. Then, data from 8–10 traverses and from adjacent ranges and bands of angles were averaged together. Finally, the observations were multiplied by range cubed to obtain a signal proportional to wave energy density. This was done because propagation loss, proportional to range to the fourth power, is partially offset by an increase in scattering area proportional to range.

The processing produced averaged maps, as a function of range and azimuth, approximately once an hour during daylight, of the energy density of receding and approaching 80 m, 7 s ocean waves out to distances of 250 km with a resolution of 7.5 km by 18°, each estimate of wave energy having a normalized standard deviation of ~20%. No observations were made at night because then signals from other LORAN stations, propagated via ionospheric paths, severely interfere with the measurements.

To collect information about other ocean waves, to obtain wave data at night, and to calibrate the radar observations, we recorded waves using wave staffs at two petroleum installations ~43 km offshore (Fig. 1a). At each installation a wave staff was suspended from a bridge connecting two platforms to minimize interference by the platforms. At one location, the staff consisted of a well-calibrated resist-

ance wire and a digital data recorder. At the second, located in the Buccaneer oil field, the instrumentation consisted of a commercial Baylor gage and analog data recorder. These have been described by Forrestall *et al.* (1977) except that for our work, data from the analog recording was digitized every 0.3 s to be compatible with data from the other installation.

Using data from the two gages, we produced estimates every 40 min of the one-dimensional frequency spectrum. These had a resolution of 6 mHz, and each point in the spectrum had the approximate statistical variability of a chi-squared distribution with 32 degrees of freedom. Typically, observations began just before the frontal passage and continued for nearly a day afterward.

c. Calibration

The radio technique makes relative measurements of wave height at different ranges and azimuths. But because of slight changes in transmitted power and unknown attenuation at different receiver locations relative to the shoreline, data from different paths and from different days cannot be directly compared. To produce a uniform set of data in absolute units of ocean-wave spectral density, all radio observations were normalized to waves recorded by the Baylor gage at the Buccaneer field. To do this, we summed the radio signal scattered from both approaching and receding waves over an arc of constant range 7.5 km wide centered at 43.1 km, an arc which includes the offshore wave gages. This sum was divided by the signals from all angles scattered from land in an arc 15 km wide centered at 45 km, on the assumption that the cross section of land targets did not vary. This removes the influence of changing transmitted power, receiver gain and transmission paths. Then, to account for the different wave heights on different days, the normalized radio cross section was divided by the strength of 80 m waves recorded at the Buccaneer field at the same time as the radio observations for all days with a signal-to-noise >4 in the ocean wave spectrum (10 observations). Finally, these ratios are averaged over all days to reduce the statistical uncertainty in the calibration coefficient relating radio scatter to ocean wave energy density in units of $m^2\ Hz^{-1}$.

The individual ratios of wave-to-land echo divided by wave energy density, for each data set, should be constant; and the observed variability was consistent with the variability in land scatter, a variability which exceeded both that of scatter from the ocean waves and that of the estimates of the wave spectra. Each ratio has an estimated normalized standard deviation of 50%, and we assume this is the uncertainty in our ability to compare radio observations of ocean waves from one day to the next, and with measurements of the ocean-wave spectral density made by others.

The above procedure relates radio scatter to wave measurements made at the Buccaneer platform. To estimate the accuracy of these wave measurements, we operated a second, calibrated resistance gage on another platform at nearly the same distance from

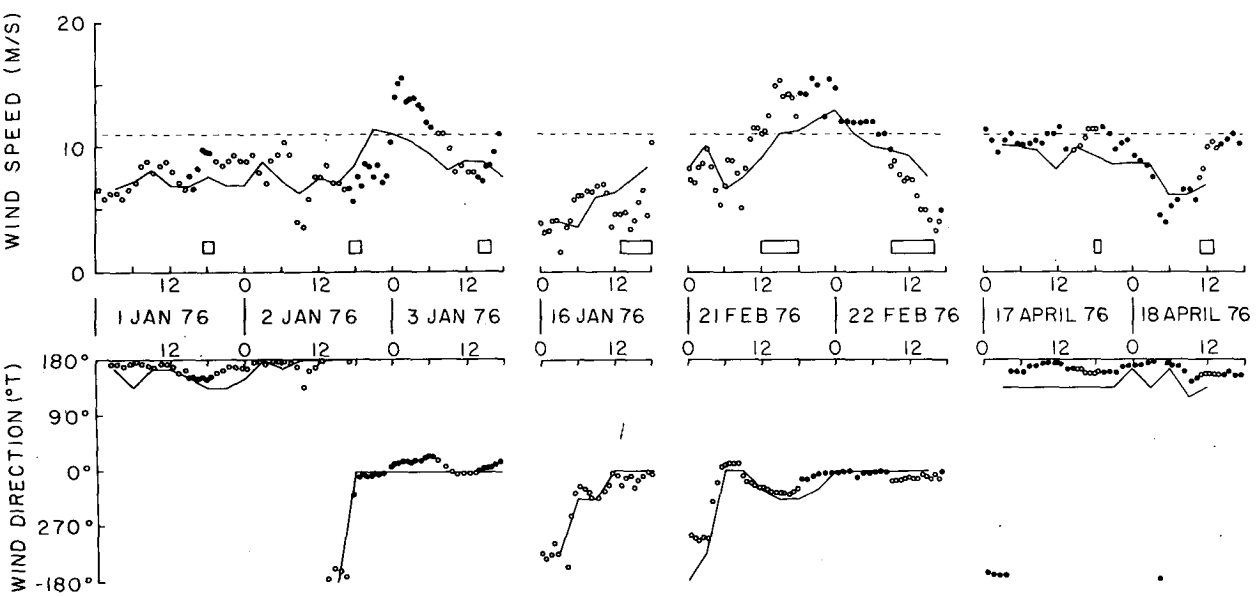

FIG. 3. Wind speed and direction measured at Buccaneer field, 43 km offshore (points) and at Galveston Island weather station (solid line). Open points are estimated from a strip chart recording of wind velocity, solid points are calculated from wind components digitized every 0.3 s and averaged over 40 min. Open rectangles are times of radar observations.

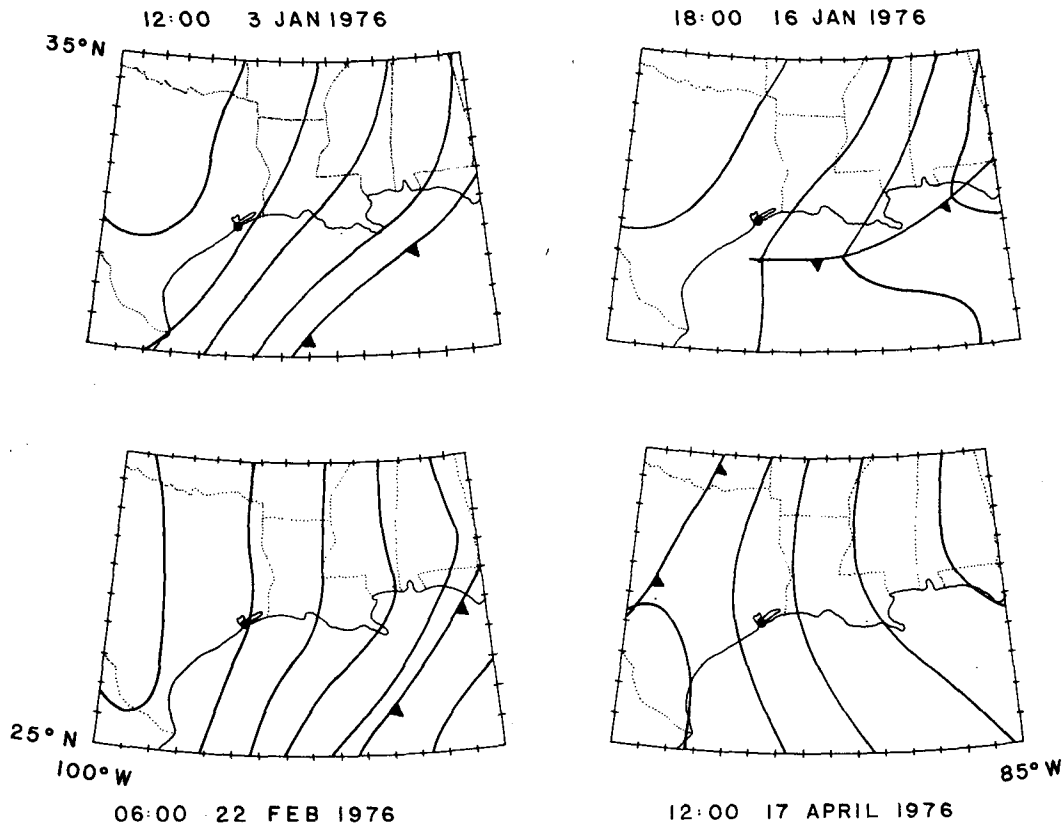

FIG. 4. Surface pressure field in the region surrounding Galveston (black dot at 29°N, 94.5°W) a few hours before radar data were collected, redrawn from U.S. National Weather Data Center analyses. Contour interval is 0.4 k Pa (4 mb), and time is Central Standard.

shore. Seven simultaneous estimates of the spectrum measured at the two platforms were compared. The spectral shapes were identical within the accuracy of the estimates and the variance of sea surface elevation, averaged over all observations, agreed within 7%.

d. Surface winds

Wind velocity was measured at the Galveston weather station, by an anemometer at the Buccaneer platform, by NOAA weather buoys and by ships further out in the Gulf. Because the Buccaneer anemometer was located over water in the radio scattering area and because it was well situated, it was the primary source of wind data for the experiment. The anemometer was 9 m above a bridge connecting two platforms and 30 m above mean sea level. Data from it were first recorded in analog form, then analyzed in two ways. Wind and wave data were digitized together and at the same rate. Vector components of the wind were averaged together to produce estimates of the mean wind vector every 40 min. In addition, a strip chart recording of wind speed and direction was produced from the analog record. The trace on the chart was averaged by eye to produce hourly estimates of the average wind vector. Both ways gave very similar estimates of the wind.

The average wind estimates at the Buccaneer field were compared with 3 h averages of the miles run by the wind in 1 h as recorded at Galveston (Fig. 3), and with 3 h estimates of the hourly observations of the octant from which the wind blew. The wind directions compared well but, as expected, wind speeds measured offshore tended to be slightly higher than those at Galveston.

To place these local observations into perspective, we obtained 6 h surface analyses of weather over North America north of 20°N from the U.S. National Weather Data Center. Maps of the regional surface pressure field approximately 6 h before waves were recorded (Fig. 4) show large-scale well-organized air flow associated with the fronts, indicating a uniform wind over the radar observation area.

e. The observation sets

Two strong fronts crossed Galveston Island in the late winter of 1976, one on 3 January 1976, the other on 22 February. On both occasions the wind

before passage of the front was southerly and sufficiently strong to generate incoming waves with a peak period near 8 s. After the fronts the winds ranged up to 15 m s^{-1}, considerably faster than the 11 m s^{-1} phase velocity of the 80 m, 7 s waves observed by the radar. These winds flattened the incoming waves and generated new waves traveling away from the coast, thus allowing us to measure the rate of wave growth with fetch as a function of angle to the wind as well as the rate of decay of the incoming waves going against the wind. A third front was observed on 16 January, but was considerably weaker than the other two.

To better understand the influence of the bottom on waves offshore of the island, we observed wind and waves on 17 and 18 April, a period of strong, steady onshore winds.

For each set of observations, we recorded radio scatter for varying periods during the daylight hours beginning just as the front passed or as the winds began to increase after passage, and continuing for the following day. Offshore, wave spectra were obtained from the Buccaneer platform beginning just before the front and continuing for 12–18 h, as well as during times radar data were collected. Winds were observed continuously for one to two days beginning just before the front passed offshore.

To summarize the spectra of ocean waves observed at the Buccaneer platform during periods of steady winds, we calculated the JONSWAP spectral parameters proposed by Hasselmann *et al.* (1973); i.e., each 40 min sample of the frequency spectrum of wave height $E(f)$ was fitted to the equation

$$E(f) = \alpha g^2(2\pi)^{-4} f^{-5} \exp[-5/4(f_m/f)^4] \times \gamma^{\exp[-(f-f_m)^2/2\sigma^2 f_m^2]}, \quad (1)$$

where f is frequency in Hertz, g is gravity, and f_m, α, γ and σ are free parameters. These parameters are listed in Table 1 for incoming waves observed just before passage of the fronts, as well as on 17 April, and for fetch-limited seas generated behind the fronts. To place these parameters in perspective, we have also included parameter calculated from the proposed scaling of α, f_m, σ and γ as a function of fetch (Hasselmann *et al.*, 1973) using the known fetch and indicated wind speed.

3. Results

a. *The effects of the bottom and observations of wave reflections*

Before considering the observations of wave growth, it is useful to test if the bottom appreciably influences wave propagation. To do this, we observed incoming waves generated by steady southeasterly winds on 17–18 April with the assumption that, on average, these waves are homogeneous. Thus we expect that the radar should observe no change in the energy density of 80 m waves traveling as a function of range along any azimuth. This expectation is supported by the observations. Using the averaged maps of radio scatter as a function of range and azimuth, we summed the scatter along arcs of constant range, and plotted the sums as a function of range for both incoming and outgoing waves (Fig. 5). The ratio scatter from incoming waves is nearly independent of range, with a slight decrease inside 40 km, and the variation in the points beyond 50 km is consistent with the statistical uncertainty in the measurement. Although not shown in the figure, the radio scatter observed as a function of range along each azimuth shows similar trends but with larger fluctuations because fewer independent points were summed together. No data are available inside of 30 km because the receiver, whose gain was set to receive distant echoes, was overloaded by the very strong transmitter pulse at short ranges. The angular spread of the 80 m waves in deep water at a range of 100 km, was 100° meas-

TABLE 1. Parameters of the ocean wave spectra observed by a wave staff 43 km offshore of Galveston.*

Time (CST)	f_m (Hz)	α	γ	σ	E (m^2)	U (m s^{-1})	θ (deg)	Comments
2 Jan 1705	0.145	0.0046	2.0	0.093	0.093			Incoming waves
3 Jan 0204	0.171	0.016	2.5	0.053	0.15	13.7	10	Fetch-limited waves
	0.173	0.013	3.3	0.080	0.18			Predicted**
0449	0.180	0.015	2.8	0.060	0.13	14.0	10	Fetch-limited waves
	0.172	0.013	3.3	0.080	0.19			Predicted
21 Feb 0359	0.145	0.0053	2.4	0.060	0.10			Incoming waves
1708	0.190	0.014	3.6	0.053	0.11	14.5	325	Fetch-limited waves
	0.190	0.014	3.3	0.080	0.14			Predicted
22 Feb 0905	0.184	0.0084	3.9	0.080	0.15	11.7	355	Fetch-limited waves
	0.194	0.013	3.3	0.080	0.11			Predicted
17 April 1505	0.110	0.0054	1.5	0.070	0.25			Incoming waves

* Parameters defined by (1).

** From mean speed and fetch in direction of mean wind using correlations given in Hasselmann *et al.* (1973).

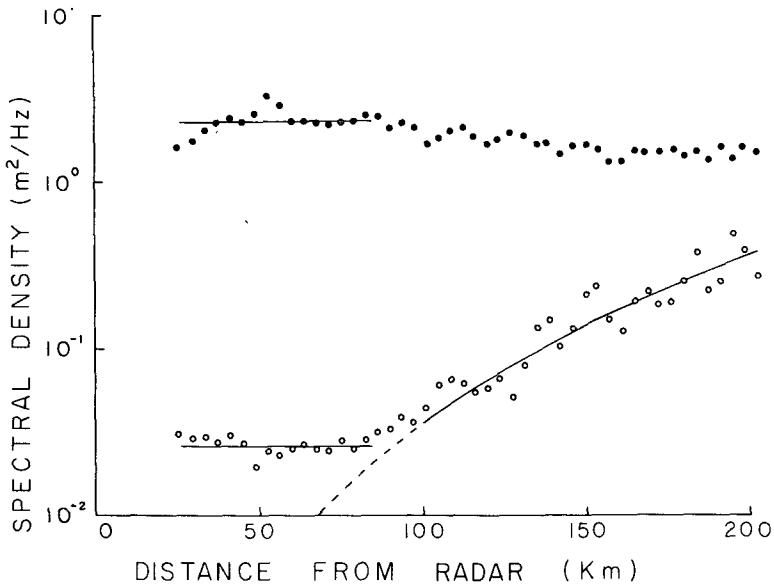

FIG. 5. Radar observations of the reflection of 80 m waves from the shore on 17–18 April. Each point is the sum of radio scatter from all directions at a fixed range and averaged over 16 traverses of the antenna path. Solid points are waves coming toward the radar, open points are receding waves. The lower line, an estimate of wave reflection, is 1% of the upper line; the curved line varies as range cubed, and is an estimate of noise beyond 100 km. Incoming waves show no influence of the bottom beyond 40 km.

ured at the half-power point and remained unchanged until the waves were within 30 km from shore, the closest we could make measurements. From this we conclude that the bottom should not appreciably influence our observations of wave growth.

As an aside, we note that the energy density of outgoing 80 m waves is also nearly constant out to ranges of 80 km, where the signal is gradually lost in noise. (The noise increases as range cubed because the radio scatter is multiplied by this factor to account for the dimunition of scattered energy with range.) The ratio of outgoing to incoming wave energy density is ~1%, and we attribute this to reflection of waves from the beach, although we discuss this observation further in Section 4d. This observed reflection coefficient is larger than might be expected from wave channel observations of reflection from beaches with shallow slope (Wiegel, 1964, p. 54), but is much less than the 20% reflection coefficient of 16 s waves incident on a steep rocky beach as measured by Munk *et al.* (1963). It is noteworthy that even very good natural beaches, such as those of Galveston Island, can reflect measurable wave energy.

b. Observations of wave growth

Wave growth was observed both as a function of time by the wave staff, and as a function of fetch by the radar. To analyze these observations we use the radiative transport equation for wave energy density (Hasselmann *et al.*, 1973)

$$\partial F(f,\theta; x,t)/\partial t + V\partial F(f,\theta; x,t)/\partial x = S, \quad (2)$$

where F is the energy density of that component of the directional spectrum of ocean waves with frequency f propagating toward θ with group velocity V; t is time, x is the distance from the radar and S is a source function.

The source function S results from the direct influence of wind blowing over the waves, from the dissipation of breaking waves, and from the interaction among components of the wave spectrum. The latter probably dominates the growth of the 80 m waves that we observed, but because we do not have good estimates of the directional spectrum of the waves over the offshore region, we have no good theoretical estimate of S, and must rely on fitting our data to an appropriate curve. Because previous measurements of wave growth have been approximated by the exponential function and because our wave observations are also well approximated by this curve (Figs. 6 and 8), we use

$$S = F\beta(f,\theta), \quad (3)$$

where β is a free parameter. This is not meant to imply that the growth is strictly exponential; indeed, other functions such as $S \propto x^n$ with $n \approx 9$ fit some of our data nearly as well although the quadratic (in time) growth proposed by Tairu (1972) did not.

Rather, we use this function so that we can directly compare our measurements with those previously reported.

Our observations fall into two classes:

(i) The radar observes the energy density $F(f_0,\theta; x,t_0)$ of fetch-limited waves measured as a function of distance and angle at a fixed time, t_0 and wave frequency f_0. Using (3) in (2) we get

$$V\partial[\ln F(f_0,\theta; x,t_0)]/\partial x = \beta(f_0,\theta). \quad (6)$$

(ii) The wave staff observes duration-limited waves integrated over all angles, at a fixed position x_0. Using (3) in (2) and integrating over θ yields

$$\partial E(f; x_0,t)/\partial t = \int_{-\pi}^{\pi} \beta(f,\theta)F(f,\theta; x_0,t)d\theta, \quad (5)$$

where

$$E(f) = \int_{-\pi}^{\pi} F(f,\theta)d\theta, \quad \overline{\zeta^2} = \int_0^{\infty} E(f)df, \quad (6)$$

and $\overline{\zeta^2}$ is the variance in sea surface elevation ζ. To simplify the integral, we write F as a product of the frequency spectrum and a directional spreading function

$$F(f,\theta) = g(f,\theta)E(f), \quad (7)$$

where $g(f,\theta)$ is normalized such that

$$\int_{-\pi}^{\pi} g(f,\theta)d\theta = 1 \quad (8)$$

to obtain

$$\partial[\ln E(f)]/\partial t = \beta(f), \quad (9)$$

where

$$\beta(f) \equiv \int_{-\pi}^{\pi} \beta(f,\theta)g(f,\theta)d\theta. \quad (10)$$

In reporting our observations, we will retain this explicit distinction between $\beta(f)$ and $\beta(f,\theta)$, not only because they are different functions, but also because there is no reason to expect that S is the same for fetch-limited waves as for duration-limited waves, but we defer until the discussion a comparison between the two. To calculate either β, we plot the logarithm of E or F as a function of x or t, and use a least-squares analysis to fit a straight line with slope $\beta(f)$ or $\beta[(f,\theta)/V]$ through the observations. Because both β's have dimension of inverse time, we divide β by f, the frequency of the wave being observed, to obtain a dimensionless measurement of wave growth.

Wave growth with fetch and angle relative to the mean wind was calculated from the radar data recorded on 3 January and 22 February 1976 at times well after passage of the front (the reason for this delay is discussed in the next section). To estimate growth rates as a function of angle, we plotted the logarithm of the energy density of 80 m waves as a function of fetch for each 18° increment in azimuth, and fitted a straight line through each set of data. Three such curves are shown in Fig. 6 and the others were very similar. Typically, 9–16 points

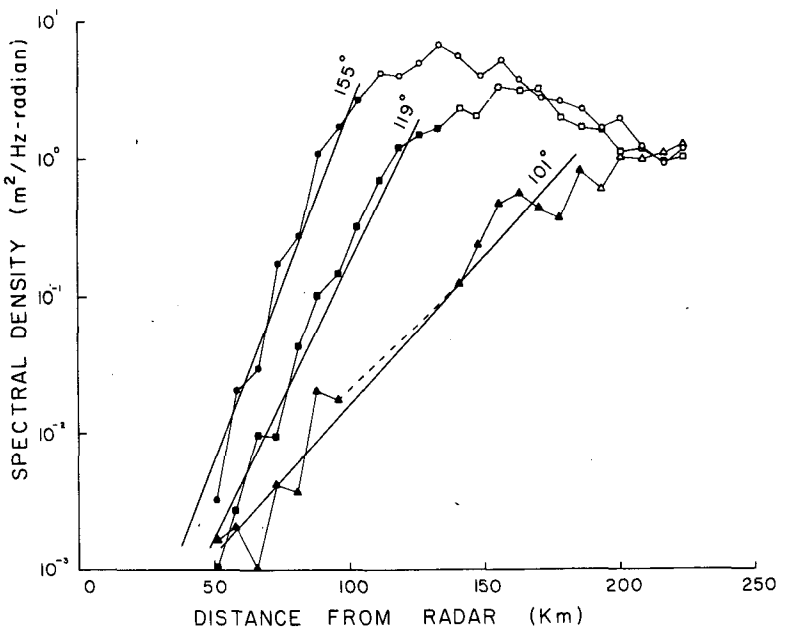

FIG. 6. Radar observations of the spectral density $F(f,\theta)$ of 80 m waves along radial lines as a function of angle θ relative to north. Data were recorded 1000–1200 on 22 February; solid points were used to determine best-fitting straight lines whose slopes yield growth rates $\beta(f,\theta)$ as a function of angle.

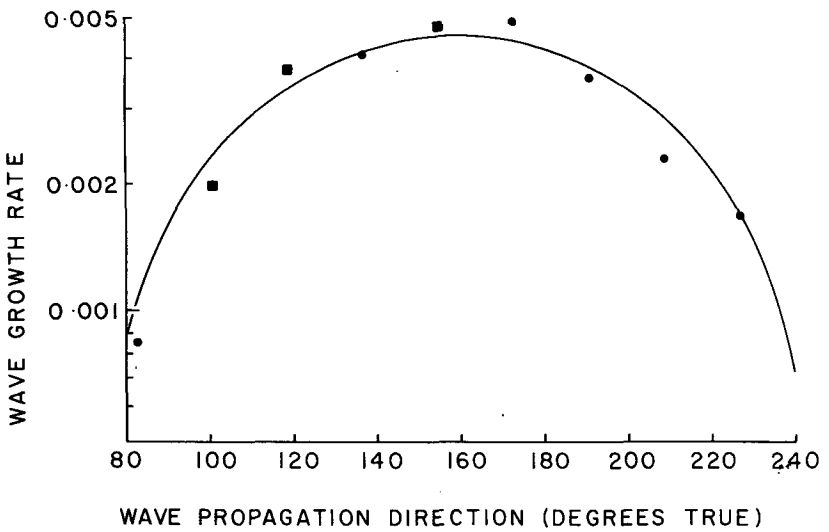

FIG. 7. Dimensionless growth rate $\beta(f,\theta)/f$ of 80 m waves observed by radar on 22 February, as a function of angle θ measured clockwise from north. The smooth curve is $0.0044\cos(\theta - 159°)$. During the time the waves were growing, the mean wind was 10.1 m s^{-1} blowing toward 165°. The solid squares are rates derived from data plotted in Fig. 6.

were used to calculate each value of $\beta(f,\theta)$, yielding least-squares fits to straight lines with correlation coefficients between 0.94 and 0.99; the best fit being to data along azimuths close to the wind direction. Wave observations at large angles to wind were much smaller and more influenced by noise. To provide a consistent measure of growth, all fitted lines extended from the smallest value of F to that value closest to one-half the maximum value of F.

These observations of $\beta(f,\theta)/f$ vs θ for the two days varied almost precisely as the cosine of the angle relative to the wind (Fig. 7). The function

$$\beta(f,\theta) = B(f)\cos^n(\theta - \theta_0) \qquad (11)$$

was fitted to the observations by minimizing the square of the difference between the observations and the curve with B, n and θ_0 as parameters. In this calculation, θ is the angle relative to north measured clockwise in degrees true; and n was restricted to 1, 2, and 4. For the observations on 3 January, we obtained $\beta/f = 0.0034\cos(\theta - 171°)$; and on 22 February $\beta/f = 0.0044\cos(\theta - 159°)$. Both values of θ_0 are within 8° of the mean wind direction averaged over the time the wind blew over the waves being measured. This was ~5 h, and is the time required for wave energy starting at the beach to reach a range of 100 km.

The temporal growth of duration-limited waves was observed using wave heights recorded as a function of time at the Buccaneer platform. From these data, we calculated wave frequency spectra $E(f)$ every 20 min and plotted the logarithm of the spectral estimates at a fixed frequency as a function of time. Again, we found that the points can be approximated by an exponential curve, but wave growth occurred very quickly and the 20 min samples barely resolve the growth. Two examples are displayed in Fig. 8. Using the slope of the lines fitted through $\ln E$ as a function of time, we calculated $\beta(f)/f$ for these waves as a function of wind speed averaged over the time waves were growing.

Our observations of $B(f)$ and $\beta(f)$ are summarized in Table 2, and are plotted in Fig. 9. Neither function shows any definite variation with wind speed

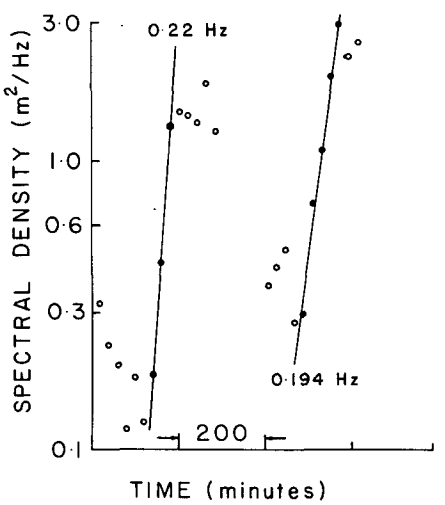

FIG. 8. Wave staff observations of the spectral density $E(f)$ of waves 43 km offshore of Galveston as a function of time at a fixed frequency. Each point is calculated from 20 min samples of wave height recorded on 21 February. Solid points were used to determine the best-fitting straight lines whose slopes yield growth rates $\beta(f)$ of these spectral components.

TABLE 2. Wave growth and decay rates.

Date 1976	Time (CST)	Data type	Frequency (Hz)	$\beta(f,0)/f \times 10^3$	$\beta(f)/f \times 10^3$	U/C
3 Jan	1420–1610	radar	0.141	3.4		0.81
2 Jan	1930–2035	staff	0.213		3.2	1.1
2–3 Jan	1705–0510	staff	0.126		−0.45	0.88
2–3 Jan	1705–0510	staff	0.132–0.145		−0.32	0.98
16 Jan	1140–1835	staff	0.11–0.17		−0.064	0.54
21 Feb	0850–1710	staff	0.132–0.145		−0.54	1.0
21 Feb	1340–1505	staff	0.194		2.3	1.5
21 Feb	1055–1140	staff	0.220		3.6	1.4
21 Feb	0605–1710	staff	0.126		−0.54	0.93
21 Feb	1210–1645	radar	0.141		−0.60	1.2
21 Feb	1705–1730	radar	0.141	3.1		1.2
22 Feb	1015–1200	radar	0.141	4.4		0.91

$\beta(f,0) = B(f)$ using (11).

U relative to wave phase velocity c, and both are nearly the same numerically.

c. *Decay of waves going against the wind and their influence on wave growth*

Onshore winds before the frontal passages generated well-developed seas that subsequently decreased in energy after the frontal passage. This decay of wave energy was observable by both the radar and the wave staff. To quantify these observations, the radar measurements of approaching 80 m waves were averaged over a band of ranges from 28.1 to 50.6 km and summed over all angles, then normalized by scatter from land. The logarithms of these values were plotted as a function of time, and the waves were found to decay approximately exponentially (Fig. 10). Again, a straight line was fitted through these data, and $\beta(f)/f$ was calculated from the slope of the line. For this calculation, only data from 21 February were useful. On 2 January the front passed through the area late in the evening, and wave decay occurred during the night when we could not make radar observations.

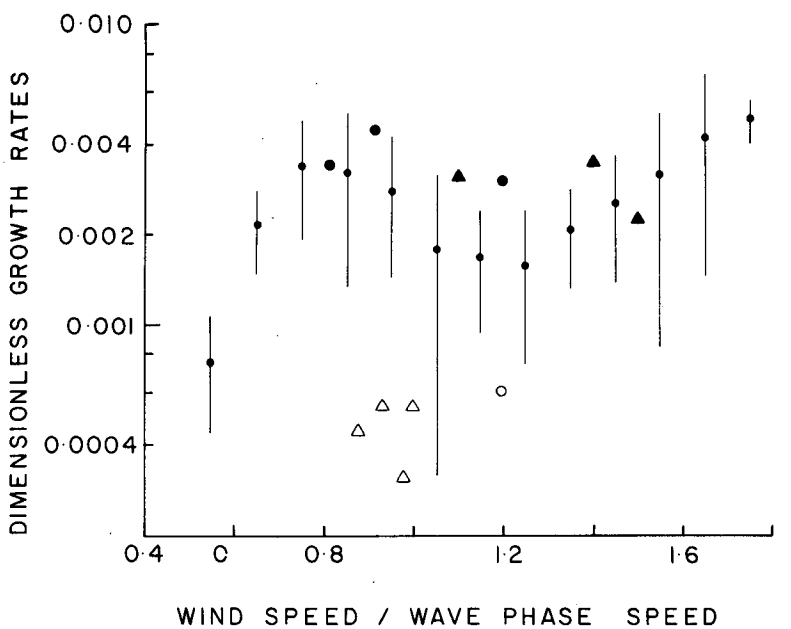

FIG. 9. Dimensionless growth (or decay) rates as a function of wind speed U divided by wave phase speed c. Small points are previously published values of $\beta(f,0)/f$ averaged over increments of 0.1 U/c; the bars are the standard deviations of these values; the solid symbols are observed growth rates of fetch-limited waves $B(f)/f$ measured by the radar (circles) and of duration-limited waves $\beta(f)/f$ measured by the wave staff (triangles). Open symbols are measurements of the decay rate $\beta(f)/f$ of waves going against the wind.

The offshore wave staff observations were processed in a similar way. Spectra were calculated every 40 min, and the logarithms of the spectral estimates near the peak in the spectrum were plotted as a function of time using data from 2–3 January, 16 January and 21–22 February 1976. Typically, 17–18 radar or wave staff observations were used to define the decay rates, and straight lines fitted through the plotted points had correlation coefficients of between 0.94 and 0.99. A typical example is plotted in Fig. 10.

We note that in the case of incoming waves, the radar and the wave staff both measure $\beta(f)$. The incoming waves are independent of fetch, and by summing the radio scatter over arcs of constant range, the radar signal is proportional to $E(f)$. When observed as a function of time, this yields $\beta(f)$. In the case of waves growing with fetch, the directional spectrum of ocean waves, defined as the angular distribution of wave directions measured at a fixed point offshore, requires the summation of radio scatter over arcs of constant range times $\sec(\theta)$, where θ is measured from the perpendicular to shore, provided the wave field does not vary in the longshore direction. This calculation requires data from great ranges to obtain data at large angles to the wind, and was not practical; thus we could not use the radar to directly observe $\beta(f)$ for the fetch-limited curves.

All rates of attenuation have been plotted as a function of wind speed relative to wave phase velocity for wind averaged over the time the waves decayed (Fig. 9). The rate of attenuation of incoming waves going against the wind is nearly independent of wind speed, and quite small. The ratio of wave decay rates to wave growth rates, averaged over all observations is 0.15. Thus wave growth rates are seven times greater than decay rates for identical wind conditions. To put these numbers into perspective, 0.139 Hz waves observed on 2–3 January required 16 h to decay to 0.1 of their initial value after passage of the front.

The slow decay of the incoming waves results in the continuing presence of large incoming waves, and this appears to inhibit the growth of waves having frequencies near the peak frequency of the incoming waves, but not at higher frequencies. For example, on 21 February the peak frequency of the incoming waves happened to coincide with that measured by the radar. Observations of the energy density of outgoing waves as a function of range, and summed over arcs of constant range (Fig. 11), shows that even 8 h after passage of the front, these waves grow for only a short distance, then remain constant. As time passed, growth increased to greater ranges; and finally, at some time between 12 and 29 h after the front passed, and after incoming waves had decayed to small values, outgoing waves

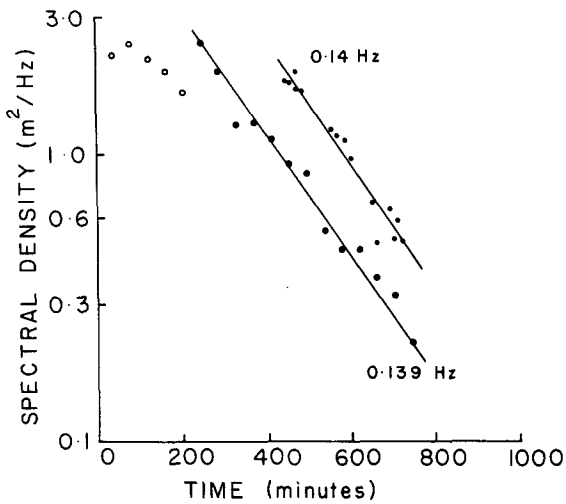

FIG. 10. Observations of the spectral density $E(f)$ of waves going against the wind (and toward the shore) as a function of time on 21 February. Small points are radar observations of $F(f,\theta)$ summed over all angles θ; large points are calculated from 40 min samples of the wave height recorded by the wave staff. The solid points were used to determine the best-fitting straight lines whose slopes yield $\beta(f)$. The origin is the same for both curves, and the vertical separation is an indication of the inaccuracy of the absolute calibration of the radar data. Both scales are identical to those in Fig. 8.

reached maximum development. Although the data are insufficient to investigate the criterion limiting wave growth, we note that the sum of approaching and receding wave amplitude (but not energy), in the region of 100 km offshore, was approximately constant.

At the same time the radar was observing this inhibition of wave growth near the peak frequency of the incoming waves, the wave staff at the Buccaneer field observed prompt growth at higher frequencies between 0.19 to 0.25 Hz (Fig. 12). This appeared as a secondary peak on the high-frequency asymptotic slope of the wave spectrum, which grew with time, and which migrated to lower frequencies. Unfortunately, because the staff was only 45 km offshore, we did not expect to observe any outgoing wave energy near 0.14 Hz, the peak frequency of the incoming waves. Waves of this frequency would only be significant beyond 100 km offshore. Thus we could not use the wave staff to observe the transition from wave decay to wave growth at the peak in the spectrum of incoming waves.

4. Discussion

a. Angular distribution of wave growth

In reporting his observations of wave growth, Fujinawa (1975) proposed that the growth rate varies as the cosine squared. In contrast, our observations are best fit by a cosine curve with but one exception. We observed that on 21 February, during times of

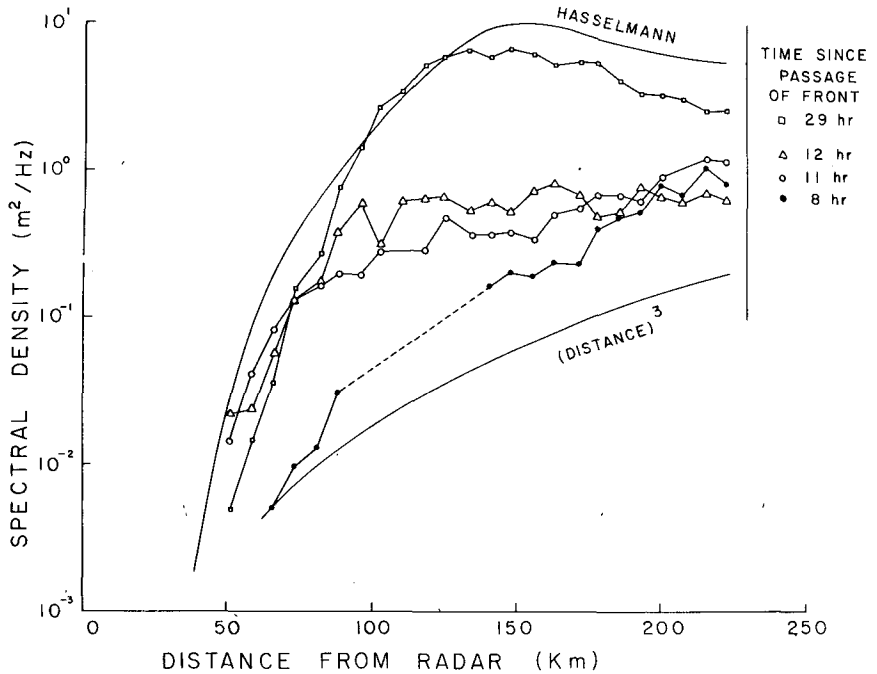

FIG. 11. Radar observations of the spectral density of fetch-limited 80 m waves as a function of range, summed over all angles (although the sum is dominated by waves within ±30° of the wind), at indicated times after passage of the front. Incoming waves appear to inhibit growth for at least 12 h, until they become small. The smooth curve, calculated from the JONSWAP spectrum (Hasselmann *et al.*, 1973) is discussed in Section 4c.

inhibited growth and while the incoming waves were still large, a cosine-squared curve seems to fit the data better; but the observations are noisy, and the correlation is only fair. Because Fujinawa also made observations immediately following the passage of a front, during times when considerable wave energy was going against the wind, his conditions closely match those of 21 February and our observations agree. But this appears to be a transitory, special condition that does not hold in general.

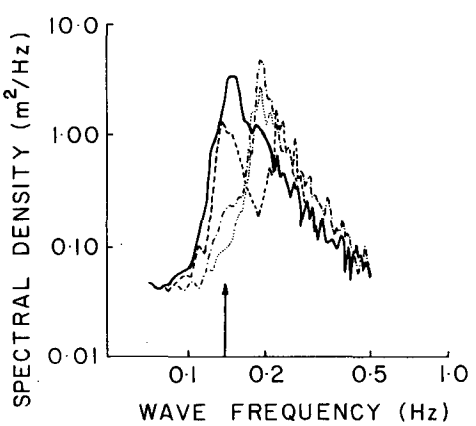

FIG. 12. The frequency spectrum of waves $E(f)$ observed as a function of time by the wave staff, showing the gradual decrease of waves going against the wind and the increase of waves (at higher frequency) going with the wind. The arrow indicates that frequency wave observed by the radar. A time history of these waves is plotted in Fig. 10. Spectra were recorded at 0358, 1135, and 1700 on 22 February, and 0905 CST 23 February.

If waves do grow as the cosine of the angle to the wind, then for winds blowing perpendicular to a straight lee shore, we infer that an initial angular distributon of wave energy density should remain unchanged or self-similar in shape during growth with fetch. That is, the variation in growth rate as a function of angle to the wind compensates for the variation of fetch with angle, so long as the waves continue to grow. Of course, once the energy density no longer scales as the cosine of the angle to the wind, the distribution of wave energy density will no longer remain self-similar.

b. Comparison of fetch-limited wave growth with duration-limited growth

In order to determine whether fetch-limited experiments might be useful in predicting the development of duration-limited seas and to compare our observations with previous measurements of growth, it is necessary to compare $\beta(f,\theta)$ with $\beta(f)$. This requires that we evaluate

$$\beta(f) = \int_{-\pi}^{\pi} \beta(f,\theta) g(f,\theta) d\theta, \qquad (12)$$

using $\beta(f,\theta)$ and $g(f,\theta)$ estimated from fetch-limited

conditions. To do this, we note that $\beta(f,\theta)$ must be small and negative for waves going against the wind if $\beta(f)$ is to be small and in agreement with our observations. Thus we can restrict the integration to $-\pi/2 < \theta < \pi/2$ with little error. Next, we use the analytic approximation to the measured values of $\beta(f,\theta)$, i.e.,

$$\beta(f,\theta) = B(f)\cos\theta, \tag{13}$$

where now θ is measured with respect to the mean wind. Finally, we assume a directional distribution of energy density in the form

$$g(f,\theta) = h\cos^n\theta, \quad -\pi/2 < \theta < \pi/2, \tag{14}$$

where h is a normalizing factor chosen to satisfy (8). This yields

$$\beta(f) = 2B(f)h\int_0^{\pi/2}\cos^{n+1}(\theta)d\theta \tag{15}$$

which has the solution

$$r = \beta(f)/B(f) = \Gamma^2\left(\frac{n+2}{2}\right)\Big/\left[\Gamma\left(\frac{n+1}{2}\right)\Gamma\left(\frac{n+3}{2}\right)\right], \quad n \geq 0. \tag{16}$$

Numerically the ratio r is bounded by 0.64 for $n = 0$ and 1.0 for $n = \infty$. Assuming $n = 2$, the value which closely fits the JONSWAP fetch-limited spectra (Hasselmann *et al.*, 1973)

$$\beta(f)/B(f) = 0.84. \tag{17}$$

Because neither the observations of $\beta(f)$ nor those of $B(f)$ show definite trends, we may be allowed to compare their mean values (denoted here by overbars): from Table 2, $\overline{\beta(f)}/f = 3.0 \times 10^{-3}$, $\overline{B(f)} = 3.6 \times 10^{-3}$, yielding $r = 0.83$. This close agreement with the calculated ratio is almost certainly fortuitous, but does indicate that, within the uncertainty in comparing $\beta(f)$ with $B(f)$, wave growth in time is numerically the same as growth in space.

c. *Comparison with previous observations of wave growth and decay rates*

Having related spatial and temporal growth rates, we can compare our observations with previous measurements of the growth rates of ocean waves. Both Barnett and Wilkerson (1967) and Synder and Cox (1966) reported measurements of $\beta(f,0)$ as a function of wind speed U relative to wave phase velocity c; and Inoue (1966) reported similarly scaled measurements of $\beta(f)$. To compare these three sets of observations, we have used the data in their figures to calculate $\beta(f,0)/f$ vs U/c so that all data are directly comparable. In particular, we used the values of β and f in Fig. 10 of Barnett and Wilkerson (solid circles) together with $U = 17.9$ m s^{-1} for the upwind data and $U = 19.5$ m s^{-1} for the downwind data. In a similar manner, we used the values of β and $W (=U)$ in Fig. 10 of Synder and Cox, together with $f = 0.313$. The data in Inoue's Fig. 1 were already in our form, except his $\ln(S_1/S_0)/(\Delta f \cdot f)$ when divided by 3600 s h^{-1} gives our $\beta(f)$. Because of the scatter in Inoue's observations, because the directional distribution of duration-limited waves is not known and because r does not differ much from 1, we have not converted his values of growth to values of $\beta(f,0)$. Rather, we have used values from his Fig. 1 without change.

The three sets of data had considerable scatter, but showed a definite trend. To summarize the values, we divided U/c into increments of 0.1 and calculated the average and standard deviation of all values of $\beta(f,0)/f$ within each increment. These are plotted in Fig. 9 together with the values of wave growth and attenuation observed offshore of Galveston Island. Our radar observations of wave growth rates yielded $B(f)$ and this is directly comparable to $\beta(f,0)$. The duration-limited growth rates $\beta(f)$ can be compared through use of (12), although (17) indicates that $\beta(f)$ differs little from $\beta(f,0)$, and the two are comparable with little error.

The most extensive measurements of fetch-limited seas were those made in JONSWAP (Hasselmann *et al.*, 1973). These were reported in the form of the spectrum (1) with parameters α, f_m, γ and σ scaled as a function of fetch and wind speed. To compare, in a rather coarse way, the radar observations with the JONSWAP observations, we used the JONSWAP form of these parameters in (1), and plotted $E(f_0)$ as a function of fetch with $f_0 = 0.14$, the frequency of waves observed by the radar, using the observed wind averaged over the time required for these waves to reach each fetch (Fig. 11). Strictly speaking, this curve of $E(f_0)$ is related to the radar measurements through a weighted integral of the directional distribution of the 0.14 Hz waves. But because the calibration of the radar data is uncertain within ±50%, such accurate comparisons are not warranted. We note only that the curve has nearly the same shape as the curve through the radar observations, and that the agreement in magnitude is within the accuracy of the measurements.

The wave staff observations provide a more accurate test of the JONSWAP spectrum, and the observed spectral parameters listed in Table 1 agree well with the values predicted from the correlations proposed in Hasselmann *et al.* (1973).

Our observations of wave attenuation can be compared with estimates used by Pierson *et al.* (1966) in their scheme for predicting ocean waves. They assume

$$F(f,\theta)/F_0(f,\theta) = \exp[-78Hf^4]^N, \tag{18}$$

where F_0 is the initial energy density of the waves, F is the energy density after they have gone against the wind for 2 h, N is a function of angle to the wind, and H is the standard deviation of surface elevation. This expression can be used with (2), together with the function form of N, to obtain

$$\beta(f,\theta) = 78Hf^4(4 - 6\theta/\pi)/7200, \quad (19)$$

where θ is the angle (rad) relative to the mean wind, and 7200 is the number of seconds in 2 h. This can be integrated in (12) if we assume

$$g(f,\theta) = 2/\pi \cos^2\theta, \quad (20)$$

a spread of wave energy density consistent with our radar observations of incoming waves (it gives a beamwidth of 90° at the half-power points compared with 100° observed by the radar). Using this yields

$$\beta(f) = (0.97)(78)(4)Hf^4/7200. \quad (21)$$

The dimension of H was never explicitly stated, but by comparing (1) in Pierson *et al.* (1966) with (12) in Pierson and Moskowitz (1964), and then rederiving the numerical example in the former, it appears that H and f have dimensions of feet and Hertz, respectively. Using $H = 0.32$ m, $f = 0.14$ Hz (typical values for incoming waves on 21 February), we obtain $\beta/f = 1.2 \times 10^{-4}$—a value slightly less than our observations of wave attenuation. Other recent, but difficult to obtain reports on wave prediction schemes use a value of 690 instead of 78 but the units are never explicitly defined. Taken at face value, this gives $\beta/f = 1.1 \times 10^{-3}$, a much greater rate of wave attenuation, and one that overpredicts the observed attenuation. Finally, we note that although (21) predicts that attenuation varies as frequency to the fourth power, we were unable to test this function. All our data are from a narrow band of frequencies, 0.10–0.14 Hz, centered about the peak in the spectrum of incoming waves. Nor could we examine $\beta(f)$ vs f/f_m, a scaling that might be expected from considerations of interactions among components of the wave spectrum.

d. Waves going against the wind

Wind-generated seas typically have wave energy propagating at large angles relative to the wind, with a significant amount of wave energy going upwind (TTSPMJ). These waves cannot be directly generated by the wind, and it is generally presumed that they are produced by wave-wave interactions which drive the wave spectrum toward an isotropic distribution. In the presence of an absorbing barrier perpendicular to the wind, a shoreline, which confines the ocean to a half plane, the upwind propagating waves are absent and must be regenerated. Observations of waves going against the wind away from such a windward shore then provides a test of wave-interaction theories, particularly that discussed by Crombie *et al.* (1978), referred to hereafter as CHS.

In an experiment nearly identical to our April measurements, CHS observed radio scatter from the sea upwind of Barbados Island, and found that the ratio of upwind to downwind traveling energy density was 1% at a range of 23 km and increased linearly to 4% at the range of 65 km for 52 m waves going against 4–11 m s^{-1} winds. They compared this observation of wave growth with that calculated from wave interactions using three models for the incoming wave spectrum: 1) J, the JONSWAP wave spectrum with $\cos^4(\theta/2)$ spreading of wave directions, where θ is the angle relative to the wind; 2) $J_{1/2}$ spectrum with $\cos^4(\theta)$ spreading; and 3) a Pierson-Moskowitz (PM) spectrum with $\cos^4(\theta/2)$ spreading. There measurements were found to be consistent with the calculations using model J.

In contrast to the Barbados observations, we failed to see waves growing against the wind, although our measurements closely duplicated those of CHS. Instead, we observed that the ratio of outgoing to incoming wave energy density was constant at ~1% out to ranges of 80 km, and did not increase with fetch. Because the energy density is constant, we identify the outgoing waves as waves reflected from the beach.

Although we failed to see waves growing against the wind, our observations do not contradict the calculations in CHS. The incoming waves have a spectrum similar to that of Pierson-Moskowitz, with a peak frequency f_m of 0.110 Hz, a small γ of 1.5, and the spread in wave directions that was slightly closer to $\cos^4(\theta/2)$ than to $\cos^4\theta$ (although $\cos^2\theta$ is perhaps better than either of these). Thus the incoming waves most closely fit model PM. If we assume a maximum linear growth rate consistent with our observations, one which gives no waves at the beach and less than 1% outgoing waves at 80 km, then our observations of waves against the wind gives an upper limit for the wave growth rate of $\beta_{CHS} = 10^5$ at $f/f_m = 1.27$ in the notation of CHS [but with the subscript to distinguish their growth rate from $\beta(f)$]. This is consistent with β_{CHS} calculated for model PM as given in their Fig. 4.

Alternatively, the difference between our observations and those of CHS may be due to Barbados being considerably less in extent perpendicular to the wind than was the Texas shoreline. This allows waves going against the wind to come around the backside of the island at angles close to those observed by the radar. Wave-wave interactions then easily diffuse this energy into angles that produce radio scatter, while at Galveston the energy must be diffused over a greater range of angle before it can be observed by the radar.

5. Conclusions

We have used a dekameter radar and wave staffs to measure waves offshore of a straight lee coast both before and after passage of strong fronts. The radar measured the growth as a function of angle to the wind of fetch-limited 80 m components of the ocean-wave spectrum; and the staff measured the temporal growth of shorter wavelengths. Both measured the decay with time of incoming winds going against the wind. We observed that growth and decay of these spectral components was approximately exponential, that growth rates varied as the cosine of the angle to the wind, and that decay rates were much smaller than growth rates under the same conditions. We also noted that while the shorter waves began to grow immediately after passage of the front, the growth of longer waves observed by the radar appeared to be inhibited by the presence of large waves which had a peak wavelength that closely coincided with the wavelength observed by the radar, and which were going against the wind. This lasted until the incoming waves decayed to small values.

The growth rates in time and space, as well as previous measurements of growth, are all related by various weighted integrals of the directional distribution of wave energy density. Fortunately, these integrals are close to unity, and the various measures of growth can be compared with little error. Within the uncertainty of the comparison and the uncertainty of the measurement, growth in time is comparable to growth in distance for those waves which we could measure, and our growth rates are comparable to previous measurements.

Because the radar was sufficiently sensitive to observe small waves going against larger waves, we could observe that ~1% of waves coming toward the beach (and generated by onshore winds) were reflected back out to sea.

Acknowledgments. This work was supported by the Office of Naval Research under Contracts N00014-75C-0356 and N00014-75C-0152. We thank Texaco, Inc., for helping us place instruments on their platform, and the Shell Development Company for providing wave and wind observations.

REFERENCES

Barnett, T. P., and J. C. Wilkerson, 1967: On the generation of ocean wind waves as inferred from airborne radar measurements of fetch-limited spectra. *J. Mar. Res.*, **25**, 292–328.

Barrick, D. E., 1972: First-order theory and analysis of MF/HF/VHF scatter from the sea. *IEEE Trans. Antennas Propag.*, **AP-20**, 2–10.

——, J. M. Headrick, R. W. Bogle and D. D. Crombie, 1974: Sea backscatter at HF: Interpretation and utilization of the echo. *Proc. IEEE*, **62**, 673–680.

Crombie, D. D., K. Hasselmann and W. Sell, 1978: High-frequency radar observations of sea waves travelling in opposition to the wind. *Bound.-Layer Meteor.*, **13**, 45–54.

Forrestall, G. F., R. C. Hamilton and U. J. Cardone, 1977: Continental shelf currents in tropical storm Delia: Observations and theory. *J. Phys. Oceanogr.*, **7**, 532–546.

Fujinawa, Y., 1975: Measurements of directional spectrum of wind waves using an array of wave detectors. Part II. Field observations. *J. Oceanogr. Soc. Japan*, **31**, 25–42.

Hasselmann, K., T. P. Barnett, E. Bouws, H. Carlson, D. E. Cartwright, K. Enke, J. A. Ewing, H. Gienapp, D. E. Hasselmann, P. Kruseman, A. Meerburg, P. Müller, D. J. Olbers, K. Richter, W. Sell and H. Walden, 1973: Measurements of wind-wave growth and swell decay during the Joint North Sea Wave Project (JONSWAP). *Erganzung. Dtsch. Hydrogr.*, Riche A, No. 12, 95 pp.

Inoue, T., 1966: On the growth of the spectrum of a wind generated sea according to a modified Miles-Phillips mechanism. New York University Geophys. Sci. Lab. Rep. TR-66-6, 64 pp. [Also see Inoue, T., 1967: On the growth of the spectrum of a wind generated sea according to a modified Mile-Phillips mechanism and its application to wave forecasting. New York University Geophys. Sci. Lab. Rep., TR-67-5, 74 pp. (Available on loan from the library, Scripps Institute of Oceanography).]

Munk, W. H., G. R. Miller, F. E. Snodgrass and N. F. Barber, 1963: Directional recording of swell from distant storms. *Phil. Trans. Roy. Soc. London*, **A255**, 505–584.

Pierson, W. J., and L. Moskowitz, 1964: A proposed spectral form for fully developed wind seas based on the similarity theory of S. A. Kitaigordskii. *J. Geophys. Res.*, **69**, 5181–5190.

——, L. J. Tick and L. Baer, 1966: Computer-based procedures for preparing global wave forecasts and wind-field analyses capable of using wave data obtained by a spacecraft. *Proc. Sixth Symp. Naval Hydrodynamics*, 499–528, Office of Naval Research ACR-122 [Gov. Printing Office, Washington, DC].

Rice, S. O., 1951: Reflection of electromagnetic waves from slightly rough surfaces. *Commun. Pure Appl. Math.*, **4**, 351–378.

Synder, R. L., and C. S. Cox, 1966: A field study of the wind generation of ocean waves. *J. Mar. Res.*, **24**, 141–178.

Sverdrup, H. U., and W. H. Munk, 1947: Wind, sea, and swell: Theory of relations for forecasting. U.S. Navy Hydrographic Office, Publ. 601, 44 pp.

Taira, K., 1972: A field study of the development of wind waves. Part I. The experiment. *J. Oceanogr. Soc. Japan*, **28**, 187–202.

Teague, C. C., G. L. Tyler and R. H. Stewart, 1977: Studies of the sea using HF radio scatter. *IEEE Trans. Antennas Propagat.*, **AP-25**, 12–18.

Tyler, G. L., C. C. Teague, R. H. Stewart, A. M. Peterson, W. H. Munk and J. W. Joy, 1974: Wave directional spectra from synthetic aperture observations of radio scatter. *Deep-Sea Res.*, **21**, 989–1016.

Wiegel, R. L., 1964: *Oceanographical Engineering*. Prentice Hall, 532 pp.